Development 136, 3007-3017 (2009) doi:10.1242/dev.037879

hnRNP I is required to generate the Ca^{2+} signal that causes egg activation in zebrafish

Wenyan Mei[1,2], Karen W. Lee[3,*], Florence L. Marlow[1], Andrew L. Miller[3] and Mary C. Mullins[1,†]

Egg activation is an important cellular event required to prevent polyspermy and initiate development of the zygote. Egg activation in all animals examined is elicited by a rise in free Ca^{2+} in the egg cytosol at fertilization. This Ca^{2+} rise is crucial for all subsequent egg activation steps, such as cortical granule exocytosis, which modifies the vitelline membrane to prevent polyspermy. The cytosolic Ca^{2+} rise is primarily initiated by inositol 1,4,5-trisphosphate (IP_3)-mediated Ca^{2+} release from the endoplasmic reticulum. The genes involved in regulating the IP_3-mediated Ca^{2+} release during egg activation remain largely unknown. Here we report on a zebrafish maternal-effect mutant, *brom bones*, which is defective in the cytosolic Ca^{2+} rise and subsequent egg activation events, including cortical granule exocytosis and cytoplasmic segregation. We show that the egg activation defects in *brom bones* can be rescued by providing Ca^{2+} or the Ca^{2+}-release messenger IP_3, suggesting that *brom bones* is a regulator of IP_3-mediated Ca^{2+} release at fertilization. Interestingly, *brom bones* mutant embryos also display defects in dorsoventral axis formation accompanied by a disorganized cortical microtubule network, which is known to be crucial for dorsal axis formation. We provide evidence that the impaired microtubule organization is associated with non-exocytosed cortical granules from the earlier egg activation defect. Positional cloning of the *brom bones* gene reveals that a premature stop codon in the gene encoding hnRNP I (referred to here as *hnrnp I*) underlies the abnormalities. Our studies therefore reveal an important new role of *hnrnp I* in regulating the fundamental process of IP_3-mediated Ca^{2+} release at egg activation.

KEY WORDS: hnRNP I, *brom bones*, IP_3, Ca^{2+}, Egg activation, Zebrafish, Cortical granule exocytosis, Maternal effect

INTRODUCTION

Egg activation ensues immediately after fertilization or egg laying, initiating a variety of cellular processes within the egg. One early event in egg activation, known as cortical granule exocytosis (CGE), modifies the vitelline membrane (also known as the zona pellucida or chorion) of the egg, and this is crucial to block polyspermy and to create a barrier to protect the developing embryo. During CGE, cortical granules (CGs), which are stimulus-dependent secretory vesicles located at the egg cortex, exocytose their contents, including enzymes and structural proteins into the perivitelline space, resulting in a permanently modified vitelline membrane (Tsaadon et al., 2006; Wassarman et al., 2001; Wessel et al., 2001).

Egg activation is initiated by a rise in cytosolic Ca^{2+}. The release of Ca^{2+} from the endoplasmic reticulum (ER) is typically triggered by fertilization and requires inositol 1,4,5-trisphosphate (IP_3) (Whitaker, 2006; Runft et al., 2002; Stricker, 1999). IP_3 is generated by activation of the phosphoinositide pathway, whereby enzymes of the phospholipase C (PLC) family cleave the lipid phosphatidylinositol 4,5-bisphosphate (PIP_2), generating IP_3. IP_3 subsequently serves as a Ca^{2+}-release messenger at egg activation to stimulate the release of Ca^{2+} from the ER (Tsaadon et al., 2006).

In zebrafish, a similar rise of cytosolic Ca^{2+} is observed upon egg activation, although egg activation in zebrafish does not require fertilization, but instead depends on a hypotonic environment, which arises when eggs are laid in normal water conditions (Hart and Fluck, 1995; Hart and Yu, 1980; Iwamatsu et al., 1997; Lee et al., 1999). As in other species, CGE in zebrafish occurs as a first response to elevated cytoplasmic Ca^{2+} levels during egg activation. CGE is required to modify the initially soft chorion, expanding and hardening it, which then serves as an important protective structure for the developing fish embryo.

We performed a maternal-effect mutant screen in the zebrafish to identify novel regulatory components of the egg activation process (Dosch et al., 2004; Wagner et al., 2004). We report here the characterization of a zebrafish maternal-effect mutant, *brom bones*, which is defective in egg activation. We show that the eggs of *brom bones* mutant females display multiple defects during egg activation, including a failure in CGE, cytoplasmic segregation, and a reduction in or absence of the Ca^{2+} wave that initiates egg activation. Providing Ca^{2+} or the Ca^{2+}-release messenger, IP_3, into *brom bones* mutant eggs rescues the egg activation defects, indicating that *brom bones* is a regulator of IP_3-mediated Ca^{2+} release. Interestingly, when the egg activation defects are incompletely penetrant, embryos from *brom bones* mutant females develop to 1 day post fertilization (dpf) and display a ventralization of the embryonic axis. Dorsal axis formation requires a cortical microtubule array that translocates a vegetally localized dorsal determinant asymmetrically to establish the dorsoventral axis. We show that in *brom bones* mutant embryos this cortical microtubule array is disorganized due to persisting, non-exocytosed CGs from earlier egg activation defects. We positionally cloned the *brom bones* maternal-effect mutant gene and found that it encodes hnRNP I, an RNA-binding protein

[1]Department of Cell and Developmental Biology, University of Pennsylvania School of Medicine, 421 Curie Boulevard, Philadelphia, PA 19104, USA. [2]The Research Institute at Nationwide Children's Hospital, Center for Cell and Developmental Biology, 700 Children's Drive, Columbus, OH 43205, USA. [3]Department of Biology, HKUST, Clear Water Bay, Kowloon, Hong Kong.

*Present address: UMR7622, CNRS/Université Pierre et Marie Curie, 9 quai St Bernard, Bat. C, 5e, 75005 Paris, France
†Author for correspondence (mullins@mail.med.upenn.edu)

Accepted 2 July 2009

belonging to the heterogeneous nuclear ribonucleoprotein (hnRNP) family. Importantly, our results demonstrate a new function for hnRNP I in vertebrate oogenesis, i.e. regulating the IP_3-mediated Ca^{2+} rise that activates the egg for zygotic development.

MATERIALS AND METHODS

In situ hybridization and immunohistochemistry

Whole-mount in situ hybridization and in situ hybridization on ovary sections were carried out essentially as described (Schulte-Merker et al., 1992; Shimamura et al., 1994). In situ probes were *boz* (Yamanaka et al., 1998), *squint* (Erter et al., 1998; Rebagliati et al., 1998), *chordin* (Miller-Bertoglio et al., 1997), *gata2* (Detrich et al., 1995), *brl* (Suzuki et al., 2000), *Vg1* (Helde and Grunwald, 1993), *mago nashi* (Pozzoli et al., 2004), *dazl* (Maegawa et al., 1999) and *brom bones* (see *brom bones* cloning).

Whole-mount antibody staining was done essentially as described (Kelly et al., 2000), using a β-catenin antibody (Schneider et al., 1996) with the ABC Kit (Vector Laboratories). To detect F-actin, rhodamine-phalloidin (Invitrogen) was used, as described (Becker and Hart, 1999). Microtubules were detected with anti-β-tubulin monoclonal antibody (Developmental Studies Hybridoma Bank) (Topczewski and Solnica-Krezel, 1999).

Cortical granules were visualized by labeling embryos with 50 μg/ml FITC-conjugated *Maclura pomifera* agglutinin (EY Laboratories, San Mateo, CA, USA). Images were taken from an MZ12.5 stereomicroscope (Leica) with a ColorSNAP-cf digital camera (Photometrics) or a Zeiss LSM510 confocal microscope, and processed using Adobe Photoshop.

Histology

Fixation of the embryos for histology, embedding in JB-4 plastic (Polysciences) and sectioning were performed as described previously (Pack et al., 1996). The sections were processed for Toluidine Blue staining (Selman et al., 1993). For electron microscopy, dissected ovaries and squeezed eggs from wild-type and *brom bones* mutant females, selected based on strong egg activation defects among their progeny, were fixed and processed according to standard protocols (Hayat, 1986). Images were captured at various magnifications using a Hamamatsu CCD camera and AMT 12-HR software.

Western blot

Western blotting was performed according to standard protocols. Antibodies used were anti-β-catenin (polyclonal, 1:1000), anti-β-tubulin (1:1000) and HPR-conjugated secondary antibodies (1:4000, Amersham). Blots were developed with the ECL Kit (Amersham).

Positional cloning of the *brom bones* gene

Mutant or wild-type sibling adult female DNA was pooled for bulk segregant analysis. Simple sequence length polymorphism (SSLP) markers were identified from the zebrafish genetic map (Shimoda et al., 1999) or generated from simple-sequence repeats found within BAC DKEY-57I11 [(CA)n1 and (CA)n2]. Open reading frames (ORFs) of candidates in BACs DKEY-57I11, DKEY-119N4 and CH211-253D24 were predicted using Genscan (http://genes.mit.edu/GENSCAN.html) and then confirmed by BLAST against the NCBI zebrafish EST database. The ORFs of the candidates were analyzed by complete sequencing of cDNAs isolated from adult mutant and wild-type ovary or brain tissue (*prg2* was only isolated from brain, as it was not detectable in the ovary). The point mutation found in the *hnrnp I* cDNA was substantiated by sequencing PCR products from genomic DNA of mutant and wild-type females, as well as the original ENU-mutagenized male from which this mutant chromosome was derived. For genotyping, genomic DNA was PCR-amplified with primers 5′-TAACATTAAACAGTCTTTAGATCGA-3′ and 5′-GCTGCCATTG-TCTGTGCATCAAAGG-3′, and digested with *Cla*I to detect a restriction fragment length polymorphism generated by the mutation. The full-length sequence of the *brom bones* transcript was further confirmed by 5′ rapid amplification of cDNA ends using the GeneRacer Kit (Invitrogen) and by sequencing ESTs that encode the *hnrnp I* transcript, CD015134 and CA470908. Full-length *hnrnp I* coding region was amplified and cloned into the CS2-MT vector to obtain pCS2-hnRNP I, to make *brom bones* antisense RNA probe.

Temperature-shift experiments

Embryos obtained from wild-type and *brom bones* mutant females were split into two groups immediately after fertilization. One subset of embryos was placed at 20°C for 2 hours and then shifted back to 28.5°C. Non-treated control groups were placed at 28.5°C. The phenotype was scored at 1 dpf.

Ca^{2+} measurements

Unactivated eggs were collected by squeezing anesthetized females and these were then injected with aequorin (supplied by Dr Osamu Shimomura) or AquaLite (Invitrogen), as described (Lee et al., 1999). Data were collected using a photon imaging microscope (PIM) as previously reported (Lee et al., 1999; Webb et al., 1997).

$CaCl_2$ and IP_3 microinjection

Unactivated eggs were collected and kept in Hank's buffered saline containing 0.5% BSA pH 7.0 to delay egg activation (Sakai et al., 1997). For Ca^{2+} injection, 2 nl of 50 mM $CaCl_2$ was injected into the center of unactivated eggs. Control eggs were injected with 50 mM KCl solution. For IP_3 injection, 2 nl of IP_3 (10 μg/μl in 125 mM KCl; BIOMOL Research Laboratories, CA-430) was injected into the center of unactivated eggs. Control eggs were injected with 125 mM KCl solution only. Following injection, eggs were kept in Hank's buffered saline containing 0.5% BSA for 15 minutes and then transferred into E3 medium for activation. Chorion elevation and cytoplasmic segregation in the injected eggs were monitored 1 hour after egg activation.

RESULTS

Embryos from *brom bones* mutant females display egg activation defects and abnormal dorsal axis formation

Embryos from *brom bones* maternal-effect mutant females (henceforth called *brom bones* mutant embryos) display two major phenotypes: a variably penetrant failure in egg activation and, in those eggs that successfully activate, a subsequent ventralization of the embryonic axis at 1 dpf (Fig. 1) (Wagner et al., 2004). A summary of the relative proportion of these two phenotypes within representative single clutches is shown in Table 1.

Egg activation in zebrafish is marked by elevation of the chorion and by segregation of the cytoplasm, which is initially integrated within the yolk, to the animal pole to form the single-cell blastodisc (Fernandez et al., 2006; Hart and Fluck, 1995). Chorion elevation is a consequence of CGE and is completed within minutes of egg activation (Becker and Hart, 1999). The chorions of *brom bones*

Table 1. Penetrance of *brom bones* mutant phenotypes

	Total number of embryos*	Embryos with egg activation defects		Ventralized embryos	Normal embryos
		Non-cellularized	Partial cellularization†		
*brb*1	62	8%	19%	23%	50%
*brb*2	69	49%	45%	6%	0
*brb*3	34	32%	26%	27%	15%

*brb*1, *brb*2, *brb*3 were three homozygous *brom bones* mutant females that are representative of the phenotypic variation seen within and between egg clutches.
*Embryos from single clutches.
†Embryos showed an enlarged yolk syncytial layer and a pocket of cells (see Fig. 1D).

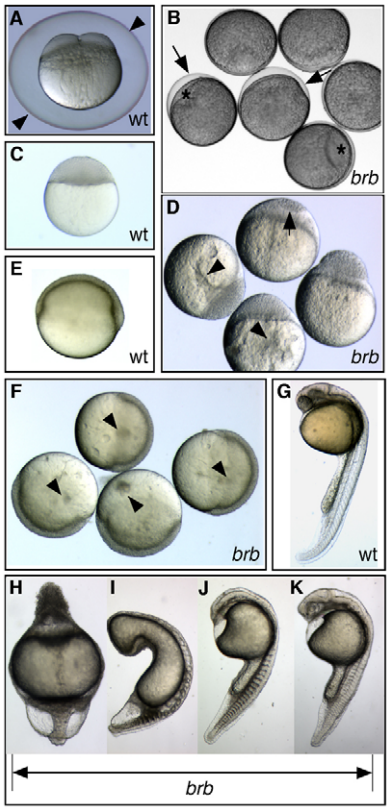

Fig. 1. *brom bones* mutants display impaired egg activation and dorsoventral patterning defects. (**A**) Wild-type (wt) 4-cell-stage zebrafish embryo at 60 mpa, with a fully elevated chorion (arrowheads). (**B**) Failed chorion elevation (arrows) and cytoplasmic segregation in *brom bones* mutant (*brb*) eggs at 60 mpa. Mutants have small blastodiscs (*) and slightly opaque yolk. (**C**) A wild-type embryo at oblong stage (a midblastula stage). (**D**) Moderately affected mutant embryos exhibit incomplete cellularization (arrow) and display large cytoplasmic inclusions in the yolk (arrowheads) at oblong stage. (**E**,**F**) Small cytoplasmic inclusions (arrowheads) are visible in the yolk of mildly affected mutant embryos (F) at gastrula stages, but not in wild-type embryos (E). (**G**) Wild-type embryo at 1 dpf. (**H**) Radially ventralized *brom bones* mutant embryo and (**I-K**) *brom bones* mutant embryos with decreasing strength of ventralization at 1 dpf. G-K are dissecting microscope images; rostral is towards the top and dorsal is to the right.

mutant eggs did not fully elevate upon egg activation (Fig. 1A,B, arrows), and remained soft rather than becoming rigid. Cytoplasmic segregation was also blocked in *brom bones* mutant eggs. Normally, cytoplasm begins to segregate from the yolk by ~10 minutes post egg activation (mpa) and is completed during early cleavage stages (Fig. 1A) (Hart and Fluck, 1995). The most strongly affected *brom bones* mutant eggs lacked obvious cytoplasmic segregation to the animal pole (Fig. 1B). Consequently, most of the cytoplasm remained in the yolk, causing the eggs to be mildly opaque, rather than becoming translucent like wild-type eggs, following cytoplasmic segregation. These *brom bones* mutant eggs had very small blastodiscs (Fig. 1B, asterisk) and showed no cell cleavage. Moderately affected eggs showed reduced and delayed cytoplasmic segregation, generating a moderately sized blastodisc at the 1-cell stage. During cleavage stages, these mutant embryos exhibited cleavage defects (Fig. 1D, arrow), displayed large cytoplasmic inclusions in the yolk (Fig. 1D, arrowheads) and died before 1 dpf. Mildly affected embryos exhibited slightly delayed and less effective cytoplasmic streaming to the blastodisc. Small cytoplasmic inclusions were apparent in the yolk of mutant embryos even during gastrula stages (Fig. 1F, arrowheads). Cellular cleavage and gastrulation appeared normal in these mildly affected embryos (Fig. 1F).

brom bones mutant embryos that were mildly affected in egg activation developed a variably penetrant ventralized phenotype at 1 dpf, as previously reported (Wagner et al., 2004). The most strongly affected embryos appeared radially ventralized, with little or no trunk development and only a few tail somites (Fig. 1H). Intermediate strength embryos lacked a notochord and displayed strongly reduced or absent head structures (Fig. 1I,J). Mildly ventralized mutant embryos exhibited a small head and eyes (Fig. 1K). The fraction of ventralized embryos from different homozygous mutant females varied (Table 1). Unaffected mutant embryos survived to adulthood (data not shown).

brom bones mutants exhibit defective CGE

We first examined the egg activation defects in *brom bones* mutants. As in other animals, CGE in zebrafish is among the first cellular responses of egg activation. CGE consists of a cascade of steps that normally complete within 5 minutes after an egg is activated. These steps include the movement of granules to the plasma membrane (PM), fusion of the CG membranes with the PM, release of the granule contents, and conclude with membrane retrieval through compensatory endocytosis (Becker and Hart, 1999; Donovan and Hart, 1986). Dynamic changes in the actin cytoskeleton are crucial to allow the CGs to fuse with the PM, and subsequently retrieve the vacant CG membrane following exocytosis (Becker and Hart, 1996; Becker and Hart, 1999; Sokac et al., 2003). Since the CGE-driven processes of chorion elevation and hardening are impaired in *brom bones* mutant eggs, we investigated whether CGE was defective by examining actin cytoskeletal dynamics.

Zebrafish eggs contain a cortical, sub-PM F-actin network that acts as a barrier to CGE prior to egg activation (Becker and Hart, 1996; Becker and Hart, 1999). Using rhodamine-phalloidin (RhPh) to label F-actin, we found that *brom bones* eggs displayed a relatively normal distribution of cortical F-actin prior to egg activation (Fig. 2A,B). Following egg activation, cortical F-actin reorganizes to allow exocytosis of CGs and then acts in compensatory endocytosis to retrieve the emptied CG membrane (CG crypt) from the egg surface. In wild-type eggs, large-scale CGE occurs within 2 mpa, which is evident by numerous patches of intense RhPh staining at the egg surface (Fig. 2C). These F-actin patches are cortical crypts at the egg surface undergoing F-actin-mediated compensatory endocytosis to retrieve the vacant granule membrane. In striking contrast, mutant eggs at 2 mpa displayed only a few patches of intense F-actin at the PM (Fig. 2D). A small number of dark circular profiles were seen on the egg surface that lacked or showed reduced RhPh fluorescence, resembling the sites where CGs are in fusion with the PM (Becker and Hart, 1999; Sokac et al., 2003). The F-actin distribution on the mutant egg surface at 2 mpa indicates that large-scale CGE is compromised in *brom bones* mutant eggs.

To determine if CGE is simply delayed or slower in *brom bones* mutant eggs, we examined F-actin organization at 5 and 30 mpa. Wild-type eggs at 5 mpa exhibited no F-actin patches and instead F-actin was distributed evenly at the egg cortex (Fig. 2E). This speckled appearance of F-actin indicates that CGE had been completed and all CG crypt membranes were retrieved by endocytosis, leaving the egg surface membrane completely

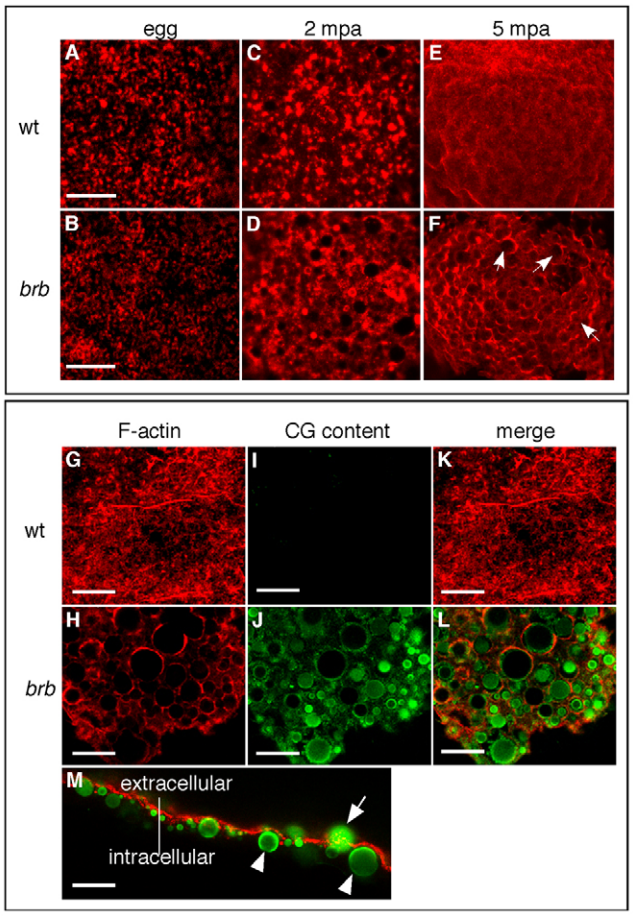

Fig. 2. CGE is defective in *brom bones* mutants. (**A**,**B**) F-actin distribution in wild-type (A) and *brom bones* mutant (B; 100%, *n*=28) zebrafish eggs prior to egg activation. (**C**,**E**) F-actin distribution in wild-type eggs at 2 (C) and 5 (E) mpa. (**D**,**F**) Abnormal F-actin distribution in *brom bones* mutant eggs at 2 (71%, *n*=35) and 5 (77%, *n*=49) mpa. The remaining mutant eggs showed F-actin distribution similar to wild-type eggs. Arrows in F highlight some of the circular profiles evident in mutant eggs. (**G-L**) F-actin (red) and CG content (green) distribution in wild-type (G,I,K) and *brom bones* mutant (H,J,L) eggs at 30 mpa (100%, *n*=71 *brom bones* mutant eggs). (**M**) Lateral view of a mutant egg surface at 5 mpa shows the localization of CG cores with respect to the F-actin meshwork. Arrow indicates a non-exocytosed granule within the F-actin meshwork; arrowheads indicate non-exocytosed granules beneath the F-actin meshwork. C-F are 20× magnification images; A-L are *z*-stacks of confocal images, M is a single confocal section. Scale bars: 10 μm in A,B; 20 μm in G-M.

remodeled (Becker and Hart, 1999; Sokac et al., 2003). In mutant eggs at 5 mpa, numerous intense circular profiles of F-actin were present on the egg surface (Fig. 2F, arrows). Surprisingly, these cortical circular profiles of F-actin persisted in mutant eggs up to 30 mpa (Fig. 2H). These circular profiles might represent non-exocytosed CGs.

To determine if CGE is blocked in *brom bones* mutants and if the circular profiles represent non-exocytosed CGs, eggs at 30 mpa were double-labeled with RhPh and FITC-conjugated *Maclura pomifera* agglutinin (MPA), which specifically labels CG contents (Becker and Hart, 1999). Indeed, the majority of circular actin profiles observed in *brom bones* mutant eggs at 30 mpa contained MPA-labeled granule contents (Fig. 2G-L). These non-exocytosed granules were located either beneath (Fig. 2M, arrowheads) or within (Fig. 2M, arrow) a cortical F-actin meshwork. These results show that in strongly affected *brom bones* mutant eggs, CGE is largely blocked, thus probably causing the failure in chorion elevation and hardening (Fig. 1A,B).

Ca^{2+} wave failure and Ca^{2+} or IP_3 rescue of *brom bones* egg activation defects

CGE is initiated by a wave of elevated cytoplasmic Ca^{2+} (Runft et al., 2002), which is triggered by interaction between IP_3 and its receptors on the ER, the intracellular Ca^{2+} storage sites. The increased cytoplasmic Ca^{2+} initiates CGE at least in part by leading to the reorganization of the cortical actin cytoskeleton barrier (Tsaadon et al., 2006). In zebrafish, a single wave of cytosolic Ca^{2+} traverses the egg during egg activation (Lee et al., 1999). CGE is accelerated when actin is depolymerized, whereas CGE is blocked when actin depolymerization is inhibited (Wolenski and Hart, 1988; Becker and Hart, 1999), suggesting that CGE is accomplished through Ca^{2+}-mediated actin reorganization. To determine if an altered Ca^{2+} wave could be the cause of impaired CGE and chorion elevation in *brom bones* mutant eggs, we examined the Ca^{2+} wave triggered at egg activation in *brom bones* eggs.

To visualize Ca^{2+} in vivo, a recombinant Ca^{2+}-sensitive bioluminescent protein was injected into the center of unactivated eggs and allowed to diffuse evenly throughout the egg for 20 minutes. The eggs were activated and bioluminescence was recorded to measure Ca^{2+} levels, followed by the acquisition of bright-field photos to examine the extent of chorion elevation (Lee et al., 1999). As shown in Fig. 3A, *brom bones* mutant eggs exhibited a defect in the increase in Ca^{2+} levels, which correlated with the extent of chorion elevation. Mutants with no detectable increase in Ca^{2+} upon egg activation exhibited no obvious chorion elevation (*n*=6 eggs), whereas mutant eggs with a small increase in Ca^{2+} showed intermediate chorion elevation (*n*=7). Mutant eggs with relatively normal Ca^{2+} levels displayed normal chorion elevation (*n*=15). These results suggest that the egg activation defects in *brom bones* mutant eggs are caused by the defective increase in Ca^{2+} levels.

To test if the defective increase in Ca^{2+} levels is the cause of the egg activation defects, we provided Ca^{2+} to *brom bones* mutant eggs and determined whether it could rescue the egg activation defects. We found that *brom bones* mutant eggs could be activated by Ca^{2+} injection, in contrast to control KCl-injected mutant eggs. In three individual experiments the percentage of activated eggs, as indicated by chorion elevation and blastodisc formation, was significantly increased in the Ca^{2+}-injected groups when compared with control groups (Fig. 3B; the bright-field live egg images show the I to V scoring series). These results indicate that defective egg activation in *brom bones* mutant eggs is caused by an impaired increase in Ca^{2+}.

We next examined whether IP_3, the major signal that releases Ca^{2+}, can rescue the *brom bones* egg activation defects. We found that *brom bones* mutant eggs could be activated by IP_3 injection, in contrast to control buffer-injected mutant eggs (Fig. 3C,D). The percentage of mutant eggs that showed both normal chorion elevation and normal blastodisc formation (data not shown) was significantly increased in IP_3-injected groups when compared with control groups (47% versus 0% in experiment 1 and 81% versus 15% in experiment 2) (Fig. 3E).

Taken together, we found that the egg activation defects in *brom bones* mutant eggs are correlated with a failure in Ca^{2+} elevation and that these defects can be rescued by providing Ca^{2+} or IP_3 to mutant

eggs prior to egg activation. These results are consistent with a model whereby insufficient IP_3 is generated in strongly affected *brom bones* mutant eggs following entry into spawning medium, causing reduced or no Ca^{2+} elevation, which leads to little or no CGE and thus a lack of chorion elevation and cytoplasmic segregation. Thus, all of the machinery downstream of IP_3 necessary for egg activation is present and functional in *brom bones* mutant eggs, but fails to be activated owing to an apparent insufficiency of IP_3.

Normal oogenesis in *brom bones* mutant females

We examined histologically and by electron microscopy the ovaries of *brom bones* mutant females to investigate whether a morphological defect in oogenesis could account for the egg activation defects. In *brom bones* mutant oocytes, CG distribution and morphology looks similar to wild-type oocytes (Fig. 4A,B, arrows). At stage IV of oogenesis, the oocyte cortex, including CGs and yolk globules, appeared similar in *brom bones* and wild-type oocytes (Fig. 4C,D). These results suggest that a gross morphological defect in oogenesis in *brom bones* mutant females does not account for the egg activation defect.

Dorsoventral axis formation in *brom bones* embryos

We next investigated the dorsoventral axis defect in *brom bones* mutant embryos. In zebrafish and *Xenopus* embryos, one of the earliest molecular steps in the establishment of the dorsoventral axis is the translocation of β-catenin, a key mediator of canonical Wnt signaling, into the nuclei of dorsal marginal blastomeres at the midblastula stage (Heasman et al., 1994; Schneider et al., 1996; Fagotto et al., 1996). Nuclear-localized β-catenin in turn acts as a transcriptional effector to activate dorsal-specific genes such as *bozozok* (*boz*; *dharma* – Zebrafish Information Network), *squint* (*ndr1* – Zebrafish Information Network) and *chordin* (reviewed by Schier and Talbot, 2005). These dorsal genes and their targets block the influence of ventralizing signals such as BMPs and promote dorsal cell fate specification (Little and Mullins, 2006).

We examined the expression patterns of dorsally and ventrally restricted genes at the beginning of gastrulation. We found that the normally dorsally localized expression of *chordin* was reduced or absent in *brom bones* mutant embryos, whereas the ventrally restricted expression of *gata2* (*gata2a* – Zebrafish Information Network) was reciprocally expanded dorsolaterally and frequently circumferentially (Fig. 5A-D′; data not shown). Further characterization showed that the dorsal defects were already apparent at sphere stage (midblastula stage) in *brom bones* mutant embryos, as indicated by the strongly reduced or absent expression of *squint* and *boz* (Fig. 5E,F, arrows; data not shown).

We then examined the nuclear localization of β-catenin in the dorsal blastomeres. We found that in *brom bones* mutant embryos, β-catenin nuclear accumulation was variably reduced and correlated with the range of ventralized phenotypes observed in mutant embryos (Fig. 5G,H; data not shown). These results indicate that dorsal axis formation in *brom bones* mutants is impaired upstream of β-catenin nuclear localization. β-catenin localization at the cell membrane of mutant embryos was as intense as in wild-type embryos, suggesting that the absence of β-catenin in dorsal blastomere nuclei of *brom bones* mutants is not due to reduced maternal β-catenin protein abundance (compare G and H in Fig. 5). We tested if normal levels of β-catenin protein were present in *brom bones* mutants and found by western blot that they were similar in

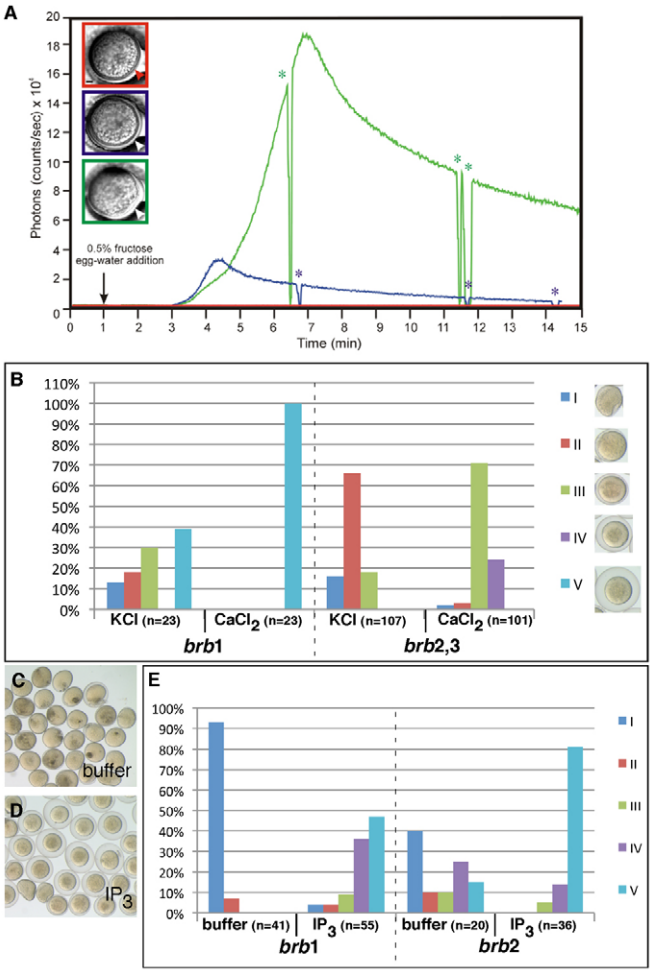

Fig. 3. Reduced Ca^{2+} wave causes egg activation defects in *brom bones* that is rescued by either Ca^{2+} or IP_3.
(**A**) Representative profiles of luminescence from aequorin-loaded zebrafish eggs (red: strongly affected *brom bones* mutant egg; blue: moderately affected mutant egg; green: mildly affected mutant egg). The profiles illustrate the total luminescent output for the entire activation process with a temporal resolution of 1 second. Arrow indicates the addition of 0.5% fructose in egg water to the egg-injection chamber to activate the eggs. Asterisks indicate the time window when the photon counting was suspended and a bright-field image of the egg was taken. Bright-field images show the egg morphology after activation, with the color of the box outline corresponding to the luminescence profile. Arrowheads indicate the degree of chorion elevation after activation. Scale bar: 100 μm. (**B**) Calcium injection rescues the egg activation defects in *brom bones* mutants. The degree of egg activation was examined after injection of KCl (control) or $CaCl_2$ into *brom bones* eggs. *brb*1, *brb*2 and *brb*3 were three *brom bones* mutant females that produced eggs in this experiment. Eggs from *brb*2 and *brb*3 showed a similar range of phenotype and rescue, and were therefore combined for simplicity. The egg activation phenotype was scored as a percentage of the total number of eggs, with the strength of egg activation divided into five classes (shown in the bright-field images, right). (**C-E**) IP_3 injection rescues the egg activation defects in *brom bones* mutants. (C,D) Eggs from a single clutch at 60 mpa after injection of buffer (C) or IP_3 (D). (E) Percentages of eggs showing different degrees of egg activation after injection of buffer or IP3. *brb*1 and *brb*2 were two mutant females that produced eggs for this experiment and are different from the females in B.

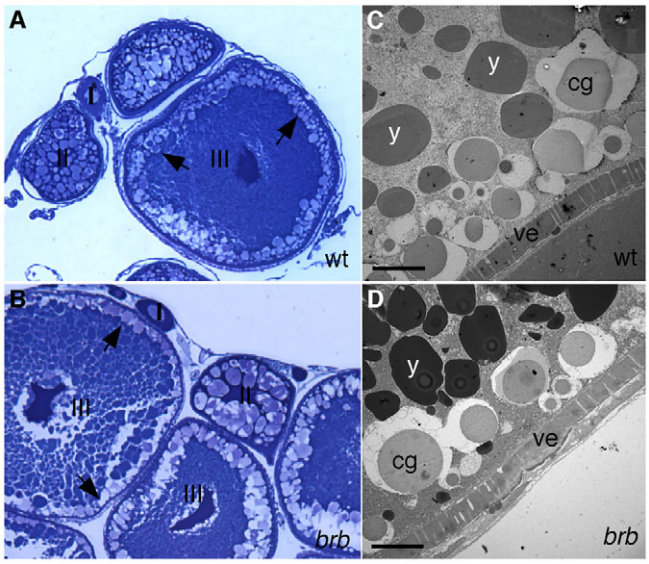

Fig. 4. Oogenesis appears normal in *brom bones* mutant females. (**A**,**B**) Stages I to III of oogenesis appear normal in *brom bones* mutant females (B, *n*=3 ovaries). Arrows indicate the location of CGs. (**C**,**D**) Transmission electron micrographs of stage IV oocytes. The morphology of cortical granules (cg), yolk globules (y) and vitelline envelope (ve) appear similar in wild-type (C) and mutant (D) oocytes. Scale bar: 10 μm.

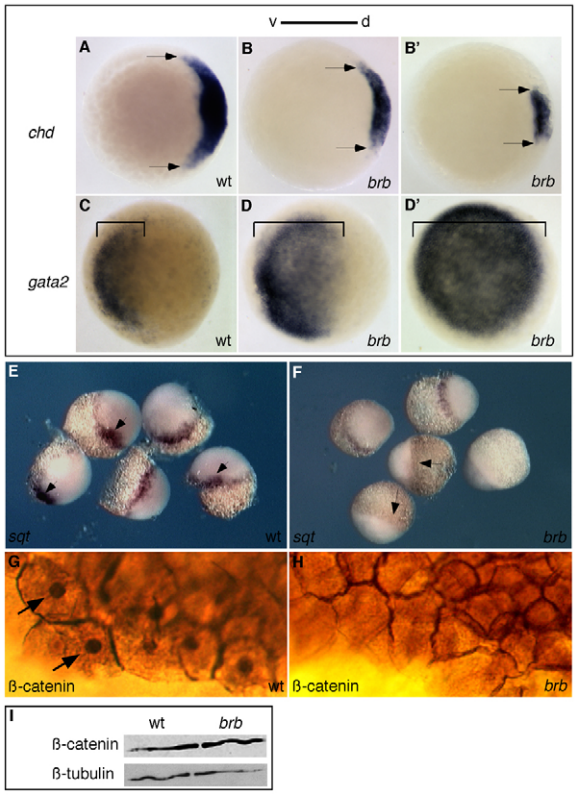

Fig. 5. Dorsal axis disruption in *brom bones* mutant embryos. (**A-F**) Dorsal gene expression is reduced and ventral gene expression is expanded in *brom bones* mutant zebrafish embryos, as revealed by whole-mount in situ hybridization. Compared with wild type (A), *chordin* is variably reduced at 50% epiboly in *brom bones* mutants (B): 24% showed moderately reduced (B), 24% showed strongly reduced (B′), 25% had absent and 27% had normal (data not shown) *chordin* expression (*n*=59). Arrows mark lateral extent of expression. (C-D′) Compared with wild type (C), *gata2* showed variable expansion in ventral tissue (denoted by brackets) in *brom bones* mutants at 50% epiboly: 25% showed partial expansion (D), 39% showed complete expansion (D′) and 36% had normal (data not shown) *gata2* expression (*n*=51). *squint* expression marks the future dorsal side at midblastula stages in wild-type embryos (E, arrows), but was absent (F, arrows; 29%), severely reduced (38%) or normal (33%, data not shown) in *brom bones* mutant embryos (*n*=45). (**G**,**H**) β-catenin protein is present in the nuclei (arrows) and at the plasma membrane in wild-type embryos (G), but was only present at the plasma membrane of *brom bones* mutant embryos (H, 29%, *n*=52). The remaining mutant embryos showed either a reduced (42%) or normal (29%) domain of nuclear-localized β-catenin (data not shown). (**I**) Western blot of 1-cell-stage lysates shows that β-catenin protein abundance was not affected in *brom bones* mutants. β-tubulin is a loading control. d, dorsal; v, ventral.

1-cell-stage mutant and wild-type embryos (Fig. 5I). Thus, we conclude that *brom bones* mutants are ventralized due to a failure in β-catenin nuclear localization in dorsal blastomeres at midblastula stages.

Disrupted cortical microtubule networks in *brom bones* embryos

In zebrafish and *Xenopus*, β-catenin nuclear translocation in dorsal blastomeres requires the asymmetric transport of a dorsal determinant at early cleavage stages via microtubules (Suprenant and Marsh, 1987; Jesuthasan and Strahle, 1997; Rowning et al. 1997; Miller et al., 1999). In zebrafish, parallel arrays of microtubules in the vegetal yolk cytoplasmic layer at the 1-cell stage and in the yolk cytoplasmic layer at early cleavage stages are required for this movement (Fig. 6A,E) (Jesuthasan and Strahle, 1997). Severe cold treatment that disrupts the cortical microtubule network prior to the 32-cell stage results in a failure of β-catenin nuclear translocation into dorsal blastomeres (Jesuthasan and Strahle, 1997). We found that the expressivity of the ventralized phenotype in *brom bones* mutants was cold sensitive. After a moderate cold treatment that does not affect wild-type embryos (0-2 hours post fertilization at 20°C), *brom bones* mutant embryos displayed a significant exacerbation in ventralization (Table 2).

Since low temperature is known to destabilize microtubules (Tilney and Porter, 1967), we asked if the microtubule networks required for dorsal determinant translocation are intact in *brom bones* mutant embryos. To address this question, whole-mount β-tubulin immunostaining was performed. Parallel arrays of microtubules were observed at the vegetal cortex of wild-type embryos at 20 minutes post fertilization (mpf) (Fig. 6B). By contrast, mutant embryos at the same stage showed variably disorganized microtubules at the vegetal pole. In the most severely affected mutant embryos, no parallel arrays of microtubules at the vegetal cortex were visible. Instead, these mutant embryos formed a short and irregular microtubule meshwork around numerous circular profiles (Fig. 6C). In intermediately affected mutant embryos, microtubule arrays appeared short at the vegetal cortex, often interrupted by the presence of circular profiles similar to those found in severely affected embryos but less abundant (Fig. 6D, arrows). Mildly affected mutant embryos showed virtually normal microtubule organization (data not shown).

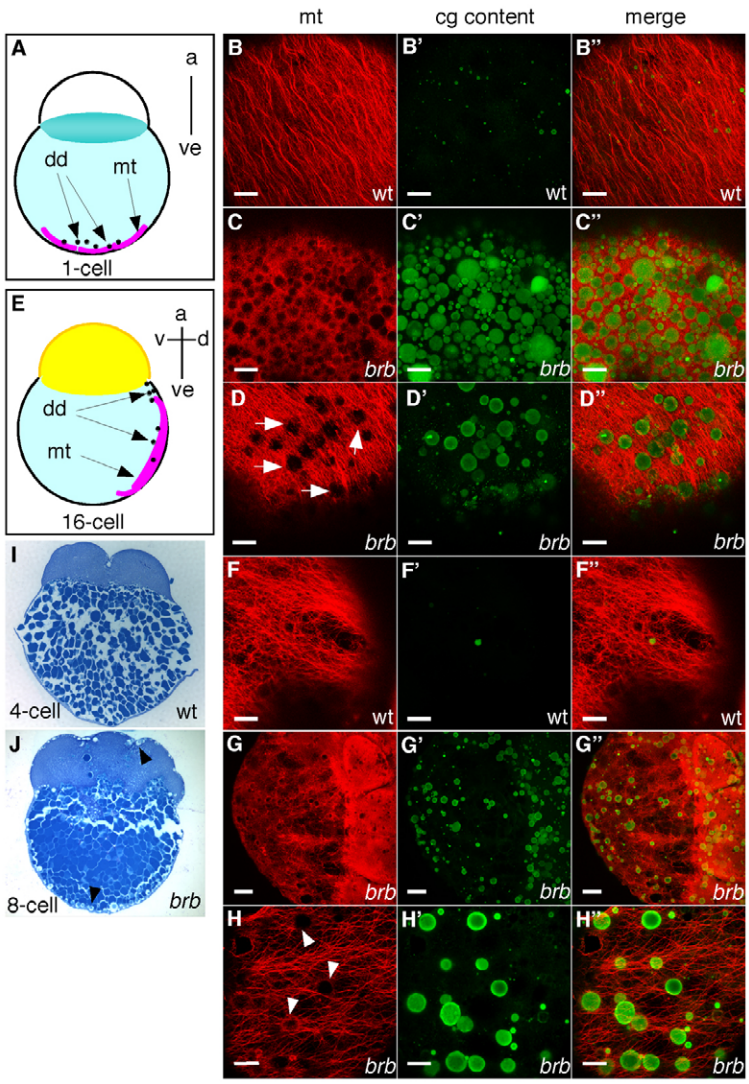

Fig. 6. *brom bones* mutants display cortical microtubule defects associated with impaired CGE. (**A**,**E**) Schematic diagrams showing parallel arrays of microtubules in the vegetal cortex at the 1-cell stage (A) and in the lateral yolk cytoplasmic layer at the 16-cell stage (E). (**B-D″**,**F-H″**) Zebrafish embryos were double-stained to show microtubules (red) and CG contents (green). Confocal image stacks of 6 μm (B-F″,H-H″) and 80 μm (G-G″). (B-D″) Embryos at 20 mpf; vegetal pole views. (B-B″) Microtubules and traces of CG content in wild-type embryos (*n*=22). Microtubules and persisting CGs in severely affected (C-C″, 16%, *n*=88) and intermediately affected (D-D″, 57%) *brom bones* mutant embryos. The remaining mutant embryos showed similar microtubule arrays to wild type (27%, data not shown). (F-H″) Embryos at the 16-cell-stage; lateral views. (F-F″) Cortical microtubules in wild-type embryos (*n*=35). (G-G″) In *brom bones* mutants the microtubule network was disrupted by circular profiles, which correspond to non-exocytosed CGs (71%, *n*=80 mutant embryos). The remaining mutant embryos showed a normal microtubule network (29%, data not shown). (H-H″) Observation at high magnification shows that the circular profiles (arrowheads) interrupting the long microtubule arrays in mutant embryos are CGs. (**I**,**J**) CGs were not observed in wild-type embryos during early cleavage stages (I), but were found in mutant embryos beneath the plasma membrane (J, arrowheads). Sagittal histological sections (5 μm) were stained with Toluidine Blue to show CGs. a, animal pole; ve, vegetal pole; d, dorsal; v, ventral; dd, dorsal determinant; mt, microtubules. Scale bars: 20 μm in B-F″,H-H″; 50 μm in G-G″.

We further examined microtubule organization in the yolk cytoplasmic layer (YCL) at the 16-cell stage. Long microtubules formed cortical arrays in wild-type embryos that extended beyond the equator (Fig. 6F). By contrast, in mutant embryos, microtubules in the YCL were sparse and failed to form arrays, due to interruption by circular profiles similar to those observed at earlier stages (Fig. 6G,H, arrowheads). The extent of microtubule disorganization in *brom bones* mutants correlated with the variation in dorsoventral patterning defects. In general, *brom bones* homozygous mutant females that produced embryos with the strongest ventralized phenotype also displayed the most severe microtubule organization defects.

Table 2. The *brom bones* dorsal axial defects are cold sensitive

Genotype	Incubation temperature (°C)	Embryos scored at 1 dpf†	Ventralized embryos			Normal embryos
			I	II	III	
Wild type*	28.5	54	0	0	0	100%
	20	91	0	0	0	100%
*brb*1	28.5	40	8%	10%	0	82%
	20	18	17%	39%	11%	33%
*brb*2	28.5	31	10%	13%	0	77%
	20	34	18%	17%	6%	59%
*brb*3	28.5	31	52%	19%	0	29%
	20	40	100%	0	0	0

I: Severely ventralized embryos were radially ventralized or headless, as shown in Fig. 1H,I.
II: Intermediately ventralized embryos displayed a partially reduced head and lacked a notochord, as shown in Fig. 1J.
III: Mildly ventralized embryos exhibited a reduced head and eyes, as shown in Fig. 1K.
*brb*1, *brb*2, *brb*3 were three homozygous *brom bones* females used in the experiment.
*Embryos from two wild-type females were scored.
†Mutant embryos that died before 1 dpf due to egg activation defects are not included in the total number of embryos scored.

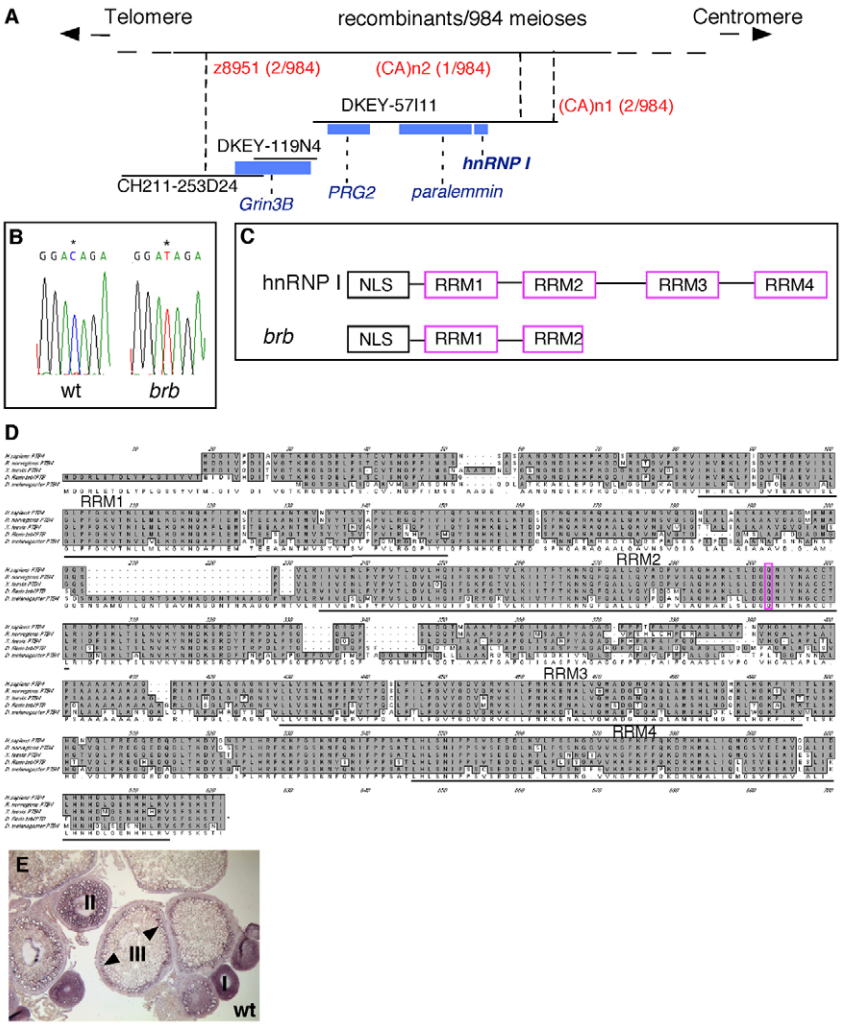

Fig. 7. Positional cloning reveals that *brom bones* encodes the RNA-binding protein, hnRNP I. (**A**) Genetic/physical map across the *brom bones* interval on chromosome 2. CH211-253D24, DKEY-119N4 and DKEY-57I11 are three sequenced and overlapping BAC clones in this interval. (CA)n1 and (CA)n2 are polymorphic markers we identified in BAC clone DKEY-57I11. Four transcription units were predicted based on the BAC sequence between z8951 and (CA)n2: *grin3b*, *prg2*, *paralemmin* and *hnrnp I*. Blue boxes indicate sizes and locations of these genes relative to the BAC clones. (**B**) Sequencing of wild-type and *brom bones* alleles revealed a cytosine to thymidine transition (*) in the open reading frame of the *hnrnp I* gene, which produces a premature stop codon. (**C**) Schematic diagram showing the protein domain structures of *hnrnp I* and *brom bones*. (**D**) Amino acid sequence alignment of hnRNP I homologs in (top to bottom) human (AAP35465), rat (Q00438), *Xenopus* (AAF00041), zebrafish (AAH95372) and *Drosophila* (NP_524703). The residue that is mutated to a stop codon in *brom bones* (purple) and the RRM domains are highlighted. (**E**) *hnrnp I* is expressed during oogenesis as revealed by in situ hybridization on wild-type ovary sections (arrowheads show cortical enrichment in stage III oocytes).

We hypothesized that the circular profiles disrupting the microtubule arrays are persistent CGs that failed to exocytose owing to the earlier egg activation defect. Indeed, persistent CGs were evident histologically in early cleavage-stage mutant embryos (Fig. 6I,J). Thus we examined the relationship between the microtubule arrays and the persisting CGs in double-labeling experiments. We found that the circular profiles that block the cortical microtubule arrays were indeed the sites of persistent CGs (Fig. 6C-D″,G-H″). These results suggest that completion of CGE is required for the proper organization of cortical microtubules acting in dorsal determinant translocation at early cleavage stages.

brom bones encodes *hnrnp I*

To better understand how *brom bones* functions, we positionally cloned the *brom bones* gene. We scanned the genome for linkage of the *brom bones* mutation to ~170 SSLP markers and found that the mutation was located between SSLP markers z9361 and z11023, close to the centromere on chromosome 2. Further analysis of 984 meioses placed the *brom bones* gene within a genetic interval of 0.3 centimorgans (cM), 0.2 cM centromeric to z8951 (two recombinants in 984 meioses) and 0.1 cM telomeric to (CA)n2 (one recombinant in 984 meioses) (Fig. 7A). This genetic interval is fully covered by three sequenced and overlapping BAC clones, which correspond to a physical interval of 248 kb between markers z8951 and (CA)n2. Using the Genscan program and the Sanger Ensembl database of zebrafish genomic sequence (www.ensembl.org), we found four transcription units within this physical interval: *glutamate receptor ionotropic NMDA 3B* (*grin3b*), *plasticity-related gene 2* (*prg2*; *fj45h08* – Zebrafish Information Network), *paralemmin* and *heterogeneous nuclear ribonucleoprotein I* (*hnrnp I*). The open reading frames of these four genes were sequenced and only a single point mutation was identified in the *hnrnp I* gene. *hnrnp I* is also known as *ptb4* (*polypyrimidine tract-binding protein 4*) (Ghetti et al., 1992; Wagner and Garcia-Blanco, 2001) and *ptbp1a*. This point mutation causes a premature stop codon in the *hnrnp I* gene (Fig. 7B). We sequenced genomic DNA from the original G0 mutagenized male fish, from which the *brom bones* mutant chromosome was derived following ENU mutagenesis (Wagner et al., 2004). We found that this parental fish did not contain the *brom bones* mutation, which excludes the possibility that this base change existed as a background polymorphism. Instead, this base change represents an ENU-induced mutation. We conclude that the *brom bones* mutant is defective in the *hnrnp I* gene.

Structurally, hnRNP I is composed of four RNA-recognition motifs (RRMs) with interdomain linker regions. Its amino-terminal extension contains both nuclear localization and export signals (Spellman et al., 2005). Zebrafish hnRNP I has the same domains as hnRNP I in other species, except that its amino-terminal extension contains 18 additional amino acids (Fig. 7C,D). The predicted protein sequence of hnRNP I shows high similarity with hnRNP I in human (75.3%),

rat (73.9%), *Xenopus* (72.2%) and *Drosophila* (46.8%) (Fig. 7D). The *brom bones* point mutation is a single nucleotide C to T transversion, converting Gln 254 to a stop codon (Fig. 7B). The mutant transcript would yield a truncated protein only containing the amino-terminal extension, the first RRM and part of the second RRM (Fig. 7C), and is therefore likely to be a strong loss-of-function mutation.

We examined the distribution of the *hnrnp I* transcript during oogenesis. *hnrnp I* is expressed throughout oogenesis. It was found throughout stage I and II oocytes, whereas in stage III oocytes it was enriched in cortical regions (Fig. 7E, arrowheads). By contrast, *hnrnp I* transcripts were not detectable in stage IV and V oocytes (data not shown).

Polarized oocyte transcript localization is unaffected

Studies in *Xenopus* oocytes show that hnRNP I is directly involved in localizing the *Vg1* transcript to the vegetal pole (Cote et al., 1999; Kress et al., 2004). To determine if hnRNP I plays a similar role in mRNA localization during zebrafish oogenesis, we examined *Vg1* (*dvr1* – Zebrafish Information Network) localization in *brom bones* mutant oocytes by in situ hybridization on ovary sections. We selected ovaries from females that consistently showed strong egg activation defects for this analysis. We found that *Vg1* transcripts were localized normally in *brom bones* mutant oocytes (data not shown). However, in zebrafish, unlike in *Xenopus* oocytes, *Vg1* RNA localizes to the animal pole rather than the vegetal pole of oocytes (Helde and Grunwald, 1993; Bally-Cuif et al., 1998). Therefore, it is possible that although hnRNP I was not required to localize animal pole transcripts, it could play a conserved role in the localization of transcripts to the vegetal pole. To test this possibility we examined three transcripts that localize to the vegetal pole, *mago nashi*, *dazl* and *bruno-like* (*brl*; *cugbp1* – Zebrafish Information Network) (Maegawa et al., 1999; Suzuki et al., 2000; Howley and Ho, 2000; Pozzoli et al., 2004; Marlow and Mullins, 2008). We found that these transcripts also localized normally in *brom bones* mutant oocytes (Fig. 8; data not shown).

The difference in hnRNP I function in transcript localization along the animal-vegetal pole in *Xenopus* versus zebrafish might be due to subfunctionalization or redundancy between multiple hnRNP I genes in the zebrafish. We recently found a second hnRNP I gene in the zebrafish genome. The second hnRNP I gene is located on chromosome 11, as a genome duplication of a small region of chromosome 2 where *hnrnp I* is located. The second hnRNP I is highly similar to *hnrnp I* (84% protein sequence identity). Since this hnRNP I gene is also expressed during zebrafish oogenesis (W.M., unpublished), it could play a role during oogenesis. Whether this second hnRNP I protein directs mRNA localization along the oocyte animal-vegetal axis will require further study.

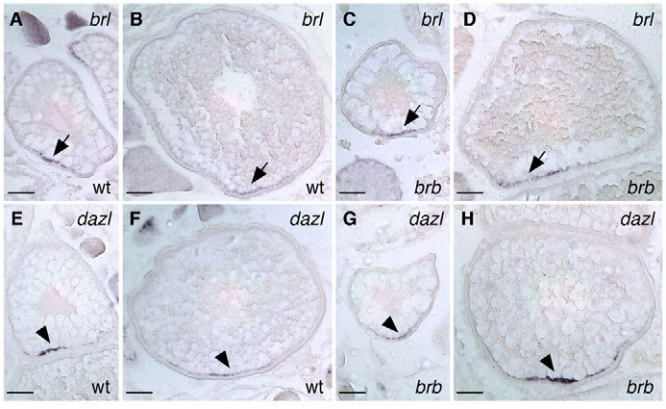

Fig. 8. Polarized RNA localization is unaffected in *brom bones* oocytes. Vegetally localized *brl* transcripts (arrows) in wild-type (**A**,**B**) and *brom bones* (**C**,**D**) zebrafish oocytes. Vegetally localized *dazl* transcripts (arrowheads) in wild-type (**E**,**F**) and *brom bones* (**G**,**H**) mutant oocytes. Stage II (A,C,E,G) and stage III (B,D,F,H) oocytes are shown. In situ hybridization was performed on sections (10 μm) of dissected ovaries. Scale bars: 50 μm.

DISCUSSION

Here we report the characterization of a zebrafish maternal-effect mutant, *brom bones*, which disrupts the *hnrnp I* gene. We show that loss of hnRNP I function impairs the Ca^{2+} wave that normally traverses the egg upon entry into spawning medium, causing a defect in egg activation, which includes impaired CGE, chorion elevation and cytoplasmic segregation. This function of hnRNP I is distinct from its previously described functions in other animals, which include roles in spermatogenesis, wing development, and RNA localization and translational regulation during oogenesis (Dansereau et al., 2002; Cote et al., 1999; Robida and Singh, 2003; Kress et al., 2004; Czaplinski and Mattaj, 2006; Lewis et al., 2008; Besse et al., 2009). Our studies reveal a new crucial role for hnRNP I in the initiation of egg activation in zebrafish.

A crucial factor in initiating egg activation at fertilization is a rise in free Ca^{2+} in the egg cytosol, although the mechanism by which Ca^{2+} evokes egg activation remains unknown. A Ca^{2+} rise in the egg cytosol upon sperm-egg fusion has been observed in virtually all animal and plant species studied, and is mediated by activation of the phosphoinositide pathway (Stricker, 1999; Runft et al., 2002; Tsaadon et al., 2006). The activated phosphoinositide pathway produces IP_3, which interacts with its receptor (IP_3R) on the ER to mediate the release of Ca^{2+}. In zebrafish, when spawning medium contacts the egg, a single Ca^{2+} wave initiates at the animal pole and traverses the egg to the vegetal pole (Lee et al., 1999). *brom bones* mutant eggs display a defect in the Ca^{2+} wave, which correlates with the strength of the egg activation defect. This suggests that failure of egg activation in *brom bones* mutants is caused by an insufficient rise in cytosolic Ca^{2+}. In support of this view, providing Ca^{2+} or IP_3 to *brom bones* mutant eggs rescues the egg activation defects. These results strongly suggest that hnRNP I plays an important role in the control of egg activation through the regulation of IP_3-mediated cytosolic Ca^{2+} release.

The IP_3 rescue data also indicate that the machinery downstream of IP_3 required for egg activation, for example the machinery required for intracellular Ca^{2+} storage and IP_3 activation of its receptor IP_3R, is intact in *brom bones* mutants. In support of this view, electron microscopy studies on unactivated *brom bones* mutant eggs suggest that the distribution and density of the ER, the major intracellular Ca^{2+} storage site in the egg cortex, are normal in *brom bones* mutant eggs (data not shown). How hnRNP I regulates IP_3-mediated cytosolic Ca^{2+} elevation then becomes an intriguing question. Since IP_3 is generated by hydrolysis of phosphatidylinositol 4,5-bisphosphate (PIP_2), hnRNP I might be required for the production of upstream activators of IP_3 at fertilization. These might include enzymes of the phospholipase C (PLC) family, as well as cytoplasmic tyrosine kinases of the Src family, which act upstream of PLC (Runft et al., 2002; Tsaadon et al., 2006). An increase of Src family activity and PLC activity upon fertilization has been observed in many organisms, including zebrafish (Wu and Kinsey, 2002; Runft et al., 2002; Kinsey et al., 2003; Sharma and Kinsey, 2006; Tsaadon et al., 2006).

hnRNP I probably regulates its target mRNA during oogenesis. Since egg activation is completed within minutes following egg laying in zebrafish, the factors involved in eliciting the Ca^{2+} wave are expected to be present as proteins in the egg, and therefore do not require mRNA translation or post-transcriptional regulation at this time. Thus, hnRNP I is unlikely to regulate its target(s) in the egg. We expect that it regulates mRNA target(s) during oogenesis, the protein product(s) of which function either directly or indirectly in activating the egg to initiate zygotic development. A possible time window for hnRNP I function is during oocyte maturation, when oocytes in most species acquire their competence to undergo egg activation-associated events, such as CGE.

brom bones mutants also display defects in dorsoventral embryonic axis formation and organization of the cortical microtubules, which are implicated in establishing the dorsoventral axis. Interestingly, the severity of microtubule organization defects correlates with the severity of the ventralization phenotype, suggesting that the former defect might be the cause of the latter. Failure to assemble contiguous microtubule arrays in the yolk cytoplasmic layer in *brom bones* mutant embryos is associated with incomplete CGE owing to the earlier egg activation defect. Incomplete CGE results in a large number of CGs remaining at the cortex of cleavage stage *brom bones* mutant embryos. These persisting CGs block the proper assembly of the cortical microtubules in eggs/embryos, which we postulate disrupt dorsal determinant translocation from the vegetal pole to the future dorsal side, and thus ventralize these embryos. However, it is also possible that *hnrnp I* regulates dorsal axis formation through an independent process. For example, it could control the IP_3-mediated cytosolic Ca^{2+} elevation during the blastula stage that is implicated in dorsal axis formation (Lyman Gingerich et al., 2005; Slusarski et al., 1997a; Slusarski et al., 1997b; Westfall et al., 2003) (reviewed by Slusarski and Pelegri, 2007). Whether *hnrnp I* regulates IP_3-mediated cytosolic Ca^{2+} elevation in different processes during zebrafish development will require further study.

Acknowledgements

We thank Tripti Gupta for helpful comments on the manuscript; Shingo Maegawa for helpful suggestions; the Penn fish facility staff (Dave Cobb, Emily Fuller, Mona Stephens-Finch, Erin Cobb) for their expert assistance; and Drs O. Shimomura, Y. Kishi and S. Inouye for supplying us with aequorin. This study was supported by grants NIH R01HD050901 to M.C.M., HKUST6416/06M and HKUST661707 to A.L.M. and by the Damon Runyon Cancer Research Foundation DRG 1826-04 to F.L.M. Deposited in PMC for release after 12 months.

References

Bally-Cuif, L., Schatz, W. J. and Ho, R. K. (1998). Characterization of the zebrafish Orb/CPEB-related RNA binding protein and localization of maternal components in the zebrafish oocyte. *Mech. Dev.* **77**, 31-47.

Becker, K. A. and Hart, N. H. (1996). The cortical actin cytoskeleton of unactivated zebrafish eggs: spatial organization and distribution of filamentous actin, nonfilamentous actin, and myosin-II. *Mol. Reprod. Dev.* **43**, 536-547.

Becker, K. A. and Hart, N. H. (1999). Reorganization of filamentous actin and myosin-II in zebrafish eggs correlates temporally and spatially with cortical granule exocytosis. *J. Cell Sci.* **112**, 97-110.

Besse, F., Lopez de Quinto, S., Marchand, V., Trucco, A. and Ephrussi, A. (2009). Drosophila PTB promotes formation of high-order RNP particles and represses oskar translation. *Genes Dev.* **23**, 195-207.

Cote, C. A., Gautreau, D., Denegre, J. M., Kress, T. L., Terry, N. A. and Mowry, K. L. (1999). A Xenopus protein related to hnRNP I has a role in cytoplasmic RNA localization. *Mol. Cell* **4**, 431-437.

Czaplinski, K. and Mattaj, I. W. (2006). 40LoVe interacts with Vg1RBP/Vera and hnRNP I in binding the Vg1-localization element. *RNA* **12**, 213-222.

Dansereau, D. A., Lunke, M. D., Finkielsztein, A., Russell, M. A. and Brook, W. J. (2002). Hephaestus encodes a polypyrimidine tract binding protein that regulates Notch signalling during wing development in Drosophila melanogaster. *Development* **129**, 5553-5566.

Detrich, H. W., 3rd, Kieran, M. W., Chan, F. Y., Barone, L. M., Yee, K., Rundstadler, J. A., Pratt, S., Ransom, D. and Zon, L. I. (1995). Intraembryonic hematopoietic cell migration during vertebrate development. *Proc. Natl. Acad. Sci. USA* **92**, 10713-10717.

Donovan, M. J. and Hart, N. H. (1986). Cortical granule exocytosis is coupled with membrane retrieval in the egg of Brachydanio. *J. Exp. Zool.* **237**, 391-405.

Dosch, R., Wagner, D. S., Mintzer, K. A., Runke, G., Wiemelt, A. P. and Mullins, M. C. (2004). Maternal control of vertebrate development before the midblastula transition: mutants from the zebrafish I. *Dev. Cell* **6**, 771-780.

Erter, C. E., Solnica-Krezel, L. and Wright, C. V. (1998). Zebrafish nodal-related 2 encodes an early mesendodermal inducer signaling from the extraembryonic yolk syncytial layer. *Dev. Biol.* **204**, 361-372.

Fagotto, F., Funayama, N., Gluck, U. and Gumbiner, B. M. (1996). Binding to cadherins antagonizes the signaling activity of beta-catenin during axis formation in Xenopus. *J. Cell Biol.* **132**, 1105-1114.

Fernandez, J., Valladares, M., Fuentes, R. and Ubilla, A. (2006). Reorganization of cytoplasm in the zebrafish oocyte and egg during early steps of ooplasmic segregation. *Dev. Dyn.* **235**, 656-671.

Ghetti, A., Pinol-Roma, S., Michael, W. M., Morandi, C. and Dreyfuss, G. (1992). hnRNP I, the polypyrimidine tract-binding protein: distinct nuclear localization and association with hnRNAs. *Nucleic Acids Res.* **20**, 3671-3678.

Hart, N. H. and Yu, S. F. (1980). Cortical granule exocytosis and cell surface reorganization in eggs of Brachydanio. *J. Exp. Zool.* **213**, 137-159.

Hart, N. H. and Fluck, R. A. (1995). Cytoskeleton in teleost eggs and early embryos: contributions to cytoarchitecture and motile events. *Curr. Top. Dev. Biol.* **31**, 343-381.

Hayat, M. A. (1986). *Principles and Techniques of Electron Microscopy: Biological Applications*, Vol. 1. New York: Litton Educational Publishing.

Heasman, J., Crawford, A., Goldstone, K., Garner-Hamrick, P., Gumbiner, B., McCrea, P., Kintner, C., Noro, C. Y. and Wylie, C. (1994). Overexpression of cadherins and underexpression of beta-catenin inhibit dorsal mesoderm induction in early Xenopus embryos. *Cell* **79**, 791-803.

Helde, K. A. and Grunwald, D. J. (1993). The DVR-1 (Vg1) transcript of zebrafish is maternally supplied and distributed throughout the embryo. *Dev. Biol.* **159**, 418-426.

Howley, C. and Ho, R. K. (2000). mRNA localization patterns in zebrafish oocytes. *Mech. Dev.* **92**, 305-309.

Iwamatsu, T., Yoshizaki, N. and Shibata, Y. (1997). Changes in the chorion and sperm entry into the micropyle during fertilization in the teleostean fish, Oryzias latipes. *Dev. Growth Differ.* **39**, 33-41.

Jesuthasan, S. and Strahle, U. (1997). Dynamic microtubules and specification of the zebrafish embryonic axis. *Curr. Biol.* **7**, 31-42.

Kelly, C., Chin, A. J., Leatherman, J. L., Kozlowski, D. J. and Weinberg, E. S. (2000). Maternally controlled (beta)-catenin-mediated signaling is required for organizer formation in the zebrafish. *Development* **127**, 3899-3911.

Kinsey, W. H., Wu, W. and Macgregor, E. (2003). Activation of Src-family PTK activity at fertilization: role of the SH2 domain. *Dev. Biol.* **264**, 255-262.

Kress, T. L., Yoon, Y. J. and Mowry, K. L. (2004). Nuclear RNP complex assembly initiates cytoplasmic RNA localization. *J. Cell Biol.* **165**, 203-211.

Lee, K. W., Webb, S. E. and Miller, A. L. (1999). A wave of free cytosolic calcium traverses zebrafish eggs on activation. *Dev. Biol.* **214**, 168-180.

Lewis, R. A., Gagnon, J. A. and Mowry, K. L. (2008). PTB/hnRNP I is required for RNP remodeling during RNA localization in Xenopus oocytes. *Mol. Cell. Biol.* **28**, 678-686.

Little, S. C. and Mullins, M. C. (2006). Extracellular modulation of BMP activity in patterning the dorsoventral axis. *Birth Defects Res. C Embryo Today* **78**, 224-242.

Lyman Gingerich, J., Westfall, T. A., Slusarski, D. C. and Pelegri, F. (2005). hecate, a zebrafish maternal effect gene, affects dorsal organizer induction and intracellular calcium transient frequency. *Dev. Biol.* **286**, 427-439.

Maegawa, S., Yasuda, K. and Inoue, K. (1999). Maternal mRNA localization of zebrafish DAZ-like gene. *Mech. Dev.* **81**, 223-226.

Marlow, F. L. and Mullins, M. C. (2008). Bucky ball functions in Balbiani body assembly and animal-vegetal polarity in the oocyte and follicle cell layer in zebrafish. *Dev. Biol.* **321**, 40-50.

Miller, J. R., Rowning, B. A., Larabell, C. A., Yang-Snyder, J. A., Bates, R. L. and Moon, R. T. (1999). Establishment of the dorsal-ventral axis in Xenopus embryos coincides with the dorsal enrichment of dishevelled that is dependent on cortical rotation. *J. Cell Biol.* **146**, 427-437.

Miller-Bertoglio, V. E., Fisher, S., Sanchez, A., Mullins, M. C. and Halpern, M. E. (1997). Differential regulation of chordin expression domains in mutant zebrafish. *Dev. Biol.* **192**, 537-550.

Pack, M., Solnica-Krezel, L., Malicki, J., Neuhauss, S. C., Schier, A. F., Stemple, D. L., Driever, W. and Fishman, M. C. (1996). Mutations affecting development of zebrafish digestive organs. *Development* **123**, 321-328.

Pozzoli, O., Gilardelli, C. N., Sordino, P., Doniselli, S., Lamia, C. L. and Cotelli, F. (2004). Identification and expression pattern of mago nashi during zebrafish development. *Gene Expr. Patterns* **5**, 265-272.

Rebagliati, M. R., Toyama, R., Fricke, C., Haffter, P. and Dawid, I. B. (1998). Zebrafish nodal-related genes are implicated in axial patterning and establishing left-right asymmetry. *Dev. Biol.* **199**, 261-272.
Robida, M. D. and Singh, R. (2003). Drosophila polypyrimidine-tract binding protein (PTB) functions specifically in the male germline. *EMBO J.* **22**, 2924-2933.
Rowning, B. A., Wells, J., Wu, M., Gerhart, J. C., Moon, R. T. and Larabell, C. A. (1997). Microtubule-mediated transport of organelles and localization of beta-catenin to the future dorsal side of Xenopus eggs. *Proc. Natl. Acad. Sci. USA* **94**, 1224-1229.
Runft, L. L., Jaffe, L. A. and Mehlmann, L. M. (2002). Egg activation at fertilization: where it all begins. *Dev. Biol.* **245**, 237-254.
Sakai, N., Burgess, S. and Hopkins, N. (1997). Delayed in vitro fertilization of zebrafish eggs in Hank's saline containing bovine serum albumin. *Mol. Mar. Biol. Biotechnol.* **6**, 84-87.
Schier, A. F. and Talbot, W. S. (2005). Molecular genetics of axis formation in zebrafish. *Annu. Rev. Genet.* **39**, 561-613.
Schneider, S., Steinbeisser, H., Warga, R. M. and Hausen, P. (1996). Beta-catenin translocation into nuclei demarcates the dorsalizing centers in frog and fish embryos. *Mech. Dev.* **57**, 191-198.
Schulte-Merker, S., Ho, R. K., Herrmann, B. G. and Nusslein-Volhard, C. (1992). The protein product of the zebrafish homologue of the mouse T gene is expressed in nuclei of the germ ring and the notochord of the early embryo. *Development* **116**, 1021-1032.
Selman, K., Wallace, R., Sarka, A. and Qi, X. (1993). Stages of oocyte development in the zebrafish, Brachydanio rerio. *J. Morphol.* **218**, 203-224.
Sharma, D. and Kinsey, W. H. (2006). Fertilization triggers localized activation of Src-family protein kinases in the zebrafish egg. *Dev. Biol.* **295**, 604-614.
Shimamura, K., Hirano, S., McMahon, A. P. and Takeichi, M. (1994). Wnt-1-dependent regulation of local E-cadherin and alpha N-catenin expression in the embryonic mouse brain. *Development* **120**, 2225-2234.
Shimoda, N., Knapik, E. W., Ziniti, J., Sim, C., Yamada, E., Kaplan, S., Jackson, D., de Sauvage, F., Jacob, H. and Fishman, M. C. (1999). Zebrafish genetic map with 2000 microsatellite markers. *Genomics* **58**, 219-232.
Slusarski, D. C. and Pelegri, F. (2007). Calcium signaling in vertebrate embryonic patterning and morphogenesis. *Dev. Biol.* **307**, 1-13.
Slusarski, D. C., Corces, V. G. and Moon, R. T. (1997a). Interaction of Wnt and a Frizzled homologue triggers G-protein-linked phosphatidylinositol signalling. *Nature* **390**, 410-413.
Slusarski, D. C., Yang-Snyder, J., Busa, W. B. and Moon, R. T. (1997b). Modulation of embryonic intracellular Ca^{2+} signaling by Wnt-5A. *Dev. Biol.* **182**, 114-120.
Sokac, A. M., Co, C., Taunton, J. and Bement, W. (2003). Cdc42-dependent actin polymerization during compensatory endocytosis in Xenopus eggs. *Nat. Cell Biol.* **5**, 727-732.
Spellman, R., Rideau, A., Matlin, A., Gooding, C., Robinson, F., McGlincy, N., Grellscheid, S. N., Southby, J., Wollerton, M. and Smith, C. W. (2005). Regulation of alternative splicing by PTB and associated factors. *Biochem. Soc. Trans.* **33**, 457-460.
Stricker, S. A. (1999). Comparative biology of calcium signaling during fertilization and egg activation in animals. *Dev. Biol.* **211**, 157-176.
Suprenant, K. A. and Marsh, J. C. (1987). Temperature and pH govern the self-assembly of microtubules from unfertilized sea-urchin egg extracts. *J. Cell Sci.* **87**, 71-84.
Suzuki, H., Maegawa, S., Nishibu, T., Sugiyama, T., Yasuda, K. and Inoue, K. (2000). Vegetal localization of the maternal mRNA encoding an EDEN-BP/Bruno-like protein in zebrafish. *Mech. Dev.* **93**, 205-209.
Tilney, L. G. and Porter, K. R. (1967). Studies on the microtubules in heliozoa. II. The effect of low temperature on these structures in the formation and maintenance of the axopodia. *J. Cell Biol.* **34**, 327-343.
Topczewski, J. and Solnica-Krezel, L. (1999). Cytoskeletal dynamics of the zebrafish embryo. *Methods Cell Biol.* **59**, 205-206.
Tsaadon, A., Eliyahu, E., Shtraizent, N. and Shalgi, R. (2006). When a sperm meets an egg: block to polyspermy. *Mol. Cell. Endocrinol.* **252**, 107-114.
Wagner, D. S., Dosch, R., Mintzer, K. A., Wiemelt, A. P. and Mullins, M. C. (2004). Maternal control of development at the midblastula transition and beyond: mutants from the zebrafish II. *Dev. Cell* **6**, 781-790.
Wagner, E. J. and Garcia-Blanco, M. A. (2001). Polypyrimidine tract binding protein antagonizes exon definition. *Mol. Cell. Biol.* **21**, 3281-3288.
Wassarman, P. M., Jovine, L. and Litscher, E. S. (2001). A profile of fertilization in mammals. *Nat. Cell Biol.* **3**, E59-E64.
Webb, S. E., Lee, K. W., Karplus, E. and Miller, A. L. (1997). Localized calcium transients accompany furrow positioning, propagation, and deepening during the early cleavage period of zebrafish embryos. *Dev. Biol.* **192**, 78-92.
Wessel, G. M., Brooks, J. M., Green, E., Haley, S., Voronina, E., Wong, J., Zaydfudim, V. and Conner, S. (2001). The biology of cortical granules. *Int. Rev. Cytol.* **209**, 117-206.
Westfall, T. A., Hjertos, B. and Slusarski, D. C. (2003). Requirement for intracellular calcium modulation in zebrafish dorsal-ventral patterning. *Dev. Biol.* **259**, 380-391.
Whitaker, M. (2006). Calcium at fertilization and in early development. *Physiol. Rev.* **86**, 25-88.
Wolenski, J. S. and Hart, N. H. (1988). Effects of cytochalasins B and D on the fertilization of zebrafish (Brachydanio) eggs. *J. Exp. Zool.* **246**, 202-215.
Wu, W. and Kinsey, W. H. (2002). Role of PTPase(s) in regulating Fyn kinase at fertilization of the zebrafish egg. *Dev. Biol.* **247**, 286-294.
Yamanaka, Y., Mizuno, T., Sasai, Y., Kishi, M., Takeda, H., Kim, C. H., Hibi, M. and Hirano, T. (1998). A novel homeobox gene, dharma, can induce the organizer in a non-cell-autonomous manner. *Genes Dev.* **12**, 2345-2353.